PRE-PRINT OF THE ARTICLE PUBBLISHED IN:
Energy Conversion and Management, Volume 164, 15 May 2018, Pages 588-602, https://doi.org/10.1016/j.enconman.2018.03.014

Exergy Analysis of Reverse Electrodialysis

F. Giacalone[a], P. Catrini[b], A. Tamburini[a], A. Cipollina[a]*, A. Piacentino[b], G. Micale[a]

[a]DIID – Dipartimento dell'Innovazione Industriale e Digitale - Ingegneria Chimica, Gestionale, Informatica, Meccanica, Università degli Studi di Palermo (UNIPA) Palermo, Italy.

[b]DEIM – Department of Energy, Information Engineering and Mathematical Models, Università degli Studi di Palermo (UNIPA) Palermo, Italy.

*Corresponding Author: andrea.cipollina@unipa.it

ABSTRACT

Reverse electrodialysis in closed loop configurations is a promising membrane technology in the energy conversion and storage fields. One of the main advantages of closed-loop reverse electrodialysis is the possibility of using a wide range of operating concentrations, flow rates and different salts for generating the salinity gradient. In this work, an original exergy analysis of the reverse electrodialysis process was carried out in order to investigate reverse electrodialysis performance in terms of energetic and exergetic efficiency parameters in a wide range of operating conditions. A mono-dimensional model of the reverse electrodialysis process was developed, in which all sources of irreversibility are considered, such as non-ideal membranes permselectivity, ohmic losses and uncontrolled mixing phenomena (salt and water diffusive flux across membranes). For each of them, the influence on the exergy efficiency is quantified and compared. Results also indicate how exergetic and energetic performance are largely dependent on solutions concentration: when high salinity gradient differences are used within the unit, membrane water permeability heavily affects process performance, thus reducing exergy efficiency, though a larger power output can be normally achieved. The more performing flow arrangement for the stack has been found to be the counter-current, though

significant differences are observed only for long channels. Finally, performance is improved when short residence time within the stack is attained for the low-concentration solution.

KEYWORDS

Salinity Gradient Power; Reverse Electrodialysis; Exergy Analysis; Chemical Exergy; Efficiency

1 INTRODUCTION

1.1 Salinity Gradient Power technologies

Energy from salinity gradients (commonly indicated as Salinity Gradient Power, SGP) is a clean and sustainable form of energy related to the mixing of solutions at different concentrations. This form of energy was described for the first time in the 1954 by Pattle [1], who also proposed how to extract it by employing Ionic Exchange Membranes (IEM). An increasing attention has been paid to this renewable energy source in the last years. In particular, in the last decade many research efforts in industry and academia have been devoted to the development of the technologies able to convert such energy into electricity. Among the different SGP technologies, reverse electrodialysis (RED) and pressure retarded osmosis (PRO) have been the most widely investigated.

In PRO [2,3], osmotic membranes are interposed between two solutions at different concentration. The difference of the chemical potential between the two solutions produces an osmotic flux from the dilute solution channel to the concentrate one. As a difference from Forward Osmosis (FO), in PRO a hydrostatic pressure lower than the osmotic pressure difference between the two channels is applied to the concentrate solution. The resulting water flux occurring from the dilute to the concentrate compartment is thus “retarded” yet pressurized.

This pressure energy gained by the permeating water is subsequently converted into electrical energy by means of a hydro-turbine coupled with a generator.

Conversely, RED allows the direct conversion of salinity gradients into electricity. RED units consist of several repetitive unit called “cell pair. A cell pair consists of two IEMs, an anion and a cation exchange membrane (AEM and CEM), interposed between two channels where the solutions at different saline concentrations flow. The chemical potential difference between the two solutions generates a selective transport of cations and anions through the membranes resulting in an ionic current and an electric potential difference over each membrane. Then, this ionic current is converted into electricity by redox reactions, which occur at two electrodes placed at the end of the cell-pairs pile.

Applications of the RED process started for the case of open-loop configuration systems, where natural salinity gradients (i.e. generated by mixing river water, seawater, brine, or brackish water) are exploited to produce electricity and after released into the environment. Several laboratory investigations have been performed and presented in literature, all focusing on how operating conditions and membrane properties can affect the main process performance parameters such as the power density and the process yield (i.e. energy generated per cubic meter of feed solutions). The first experiments related to RED process were carried-out in 1954 and reported a power density of 0.05 W/m^2 [1]. Several years later almost one order of magnitude higher values (i.e. 0.4 W/m^2) were found by Audinos [4] in 1983 and a further doubling (about 0.93 W/m^2) was reported by Veerman et al. [5]. The power density obtainable from these early tests was limited due to the lack of suitable IEMs. Only during the last decade, the development in membrane fabrication technology and stack design as well as the adoption of specific operating conditions [6,7] allowed significantly higher power density values to be obtained. For instance, power densities up to 6.7 $W/m^2_{membrane}$ [8] were found using high salinity solutions (e.g. brines) and higher temperatures (e.g. 60°C). All these extensive research efforts

have recently led to the successful design and operation of the first pilot scale prototypes fed with natural salinity gradients in real environment [9,10].

RED technology has been investigated also in a closed-loop configuration, with the aim to convert low-grade waste heat into electricity. This innovative *Reverse Electrodialysis-Heat Engine* (RED-HE) [11] consists of a traditional RED unit coupled with a Thermal Regeneration Unit (TRU). The TRU is provided with waste heat, which is used in a purposely-selected thermally-driven process to restore the initial concentrations of the solutions exiting from the RED unit. In this way the regenerated solutions can be fed again to the RED unit, thus closing the cycle. These systems could be profitably coupled to several industrial processes, like manufacturing or metallurgical industries, where low-grade waste heat is discarded into the environment. In this way, a reduction of fossil fuel consumptions could be achieved with economic and environmental benefits.

One of the most significant features of the RED-HE process is that there is no need for natural salinity gradients sources, thus overcoming the main restriction of implementation of the RED process which is obviously limited only to those sites where natural sources of SGP are available. The RED-HE can be in fact implemented in principle anywhere, thanks to the use of a limited quantity of artificial saline solutions suitably-selected for optimal process performance [12,13].

Another interesting application of closed-loop reverse electrodialysis systems is the development of a “salinity gradient based battery”. Some examples of this application have been proposed so far both in scientific papers [14,15] and high-risk cooperation projects [16]. Both in open- and closed-loop configuration the enhancement of energy performance of RED units is a matter of crucial importance.

1.2 Exergy Analysis

Exergy analysis represents a powerful method to identify the main sources of energy loss and quantify how much energy is effectively converted within the process. While in open-loop RED applications the process yield (i.e. how much energy is generated from the available salinity gradient) is the most important parameter, in closed-loop applications the efficiency of salinity gradient conversion dominates the overall process efficiency. In fact, only a part of the available salinity gradient is reversibly converted into electricity, while the remaining is dissipated without producing energy, yet requiring additional effort in the regeneration stage. With this respect, exergy analysis can be very useful to drive stack design and identify optimal operating conditions. Kotas in 1985 [17] defined the exergy of a system as "*the maximum amount of work obtainable when it evolves from its thermodynamic state to the thermomechanical and chemical equilibrium with the environment through reversible processes involving mass and heat transfer between the system and the environment*". Differently from energy, exergy is destroyed in real systems operation due to irreversible phenomena like heat exchange, uncontrolled mixing, friction or chemical reactions [17]. The assessment of exergy destruction due to irreversibility occurring within each component of a cycle provides fundamental information on the main limiting factors of the entire cycle, identifying possible design and operative improvements, in order to achieve profitable energy conversion and/or savings [18].

In scientific literature, exergy analysis has been extensively applied to the study of several "energy systems" performance. Sun et al. [19] carried out an exergy analysis to support Organic Rankine Cycle (ORC) systems design. Ranjbar applied the energy and exergy analysis (method) to the design of a novel trigeneration system based on a solid oxide fuel cell [20]. Other researches have been focused on cryogenic process as natural gas liquefaction [21], energy recovery in natural gas compressor station [22] and steam power plant [23], air treatment for heating, ventilation, air conditioning (HVAC) systems [24] and the design of controllers in refrigeration system [25]. Exergy analysis has been also applied to membrane [26,27] and

thermal [28,29] desalination processes. Conventional exergy analysis identifies and quantifies irreversibility sources, though it does not allow to evaluate the economic and environmental benefits that may arise by their reductions [30]. To this aim, more complex and refined exergy-based approaches have been proposed during these years. For instance, thermo-economics [31] combines exergy analysis with economic principles to provide criteria for costs allocation in energy system [32] or for optimization of the design and operation of energy systems [33] and to support diagnosis malfunction in thermal energy systems [34]. Exergy can also be used to assess the quality and the consumption of natural resources burdening a given product [35]. To this aim, Cornelissen et al. [36] combine exergy analysis with Life Cycle Assessment framework, i.e. Exergy Life Cycle Assessment (ELCA), to evaluate the usage of non-renewable exergy occurring along the entire life of a product. A further evolution of the ELCA approach was presented in [37] and integrates the well-known Input-Output analysis into ELCA, through the use of the Monetary Input Output Tables (MIOTs) of national economies. An example of application of this alternative approach is presented in 2016 by Rocco et al. [38], who assessed the primary non-renewable exergy embodied in electricity produced by a Waste-to-Energy power plant operating in the Italian context.

1.2.1 *Exergy analysis of RED*

In a RED process, exergy variations of the feed streams occur due to the variation in solutions composition within the unit. Only if the process is operated reversibly, exergy would be entirely converted into electric power. In real cases, some detrimental phenomena inevitably occur there by contributing to reduce the exergy performance of RED units. Irreversibility sources involved in the RED process are summarized in Table 1.

The non-ideal behaviour of IEMs is responsible for uncontrolled mixing effects (i.e. water and salt diffusion), which reduce part of the available driving force, consuming part of the exergy content of the inlet streams without producing electrical power. Non-ideal IEMs

permselectivity also affects the generated electromotive force, which is reduced with non-unitary permselectivity. Furthermore, membrane and solution resistances are also significant causes of exergy destruction (i.e. internal ohmic losses). Other sources of irreversibility are the friction losses inside the channels, the activation losses in the electrodic compartments and the parasitic currents in the distribution manifolds. However, friction losses are dramatically dependent on channels configuration (not considered in this study) and the latter two losses have a minor role in the overall process exergy performance and have been thus neglected in the present work.

Table 1. Description of the irreversibility sources involved in the RED process.

Irreversibility source	Description
Permselectivity	Exergy destruction due to the non-ideality of the IEMs, which affects interface equilibria, thus also reducing the electro-motive force and the overall generated stack voltage.
Ohmic losses	Exergy destruction due to the power dissipated due to the internal stack resistance
Water flux	Exergy destruction associated to the water flux across the IEMs which reduces the available salinity gradient for power production.
Salt flux	Exergy destruction associated to the salt flux across the IEMs which reduces the available salinity gradient for power production.
Friction losses & pumping power	Exergy dissipated for flowing of the solutions within the channels.
Parasitic currents	Exergy destruction due to the generation of parasitic currents through the stack which dissipating part of the electrical energy generated inside the system
Activation losses	Exergy destruction due to the electrical potential drops often related to redox reactions in the electrodic compartments (smaller with reversible redox couples, as in the present case).

Few research efforts have been devoted so far to thermodynamic analysis of RED units. Veerman et al. [39] pointed out the crucial role played by membrane properties on energy performance. On the basis of an ideal model for thermodynamic properties estimation, they

experimentally analysed the thermodynamic efficiency and power densities of a RED unit equipped with six commercial membranes, reporting thermodynamic efficiency between 14% and 35%. They also demonstrate that the non-ideal behaviour of the membranes is due to osmosis and co-ion transport and that loss in efficiency due to osmosis is small compared to co-ion. The same authors in [40] developed a 1-D model for the RED unit, which introduced the exergy concept. The model was calibrated with experimental data and used to study response parameters, suitable for optimization purposes. It was found that performance of co-current and counter-current operation is almost identical and that segmentation of the electrodes can increase the power density with about 15%. Yip et al. [41] proposed a model to assess the production of work respectively in a reversible and real RED process. The model defines suitable dimensionless parameters, which have to be properly assessed according to the type of membrane and operating conditions considered. By thoughtful selection of the operating parameters they achieved a thermodynamic efficiency of 37% and an overall gross power density of 3.5 W/m^2 with seawater-river water RED system with low-resistance ion exchange membranes (0.5 cm^2) at very small channels thickness (50 μm). Vermaas et al. [42] investigated the effects of different flow arrangements, single and multi-electrodes configurations on the energy efficiency of RED unit equipped with perfect membranes. They reported a maximum energy efficiency of 95% when using seawater and river water flowing in counter-current arrangement.

1.3 Aim of the work

Most of the works reported in literature limited their investigation to the case of seawater and river water as it is the most common natural salinity gradient. Conversely, a variety of artificial solutions could be in principle used in closed-loop applications, leaving large room for further studies. Moreover, literature works typically refer to thermodynamic efficiency (or energy

efficiency) as performance indicator, while exergy efficiency is not mentioned or not properly quantified in any study.

For the first time, in this work, exergy analysis is extensively applied to a RED process to identify the main sources of irreversibility and quantifying their detrimental effect on process performance. The analysis was supported by a robust 1-D model for the description of all the transport phenomena within the RED unit assuming real membrane properties. The effect of each IEM property (i.e., permselectivity, water and salt permeability, and resistance) is quantitatively identified, providing relevant information for orienting future development of better performing IEMs. As a matter of fact, some detrimental effects as the water flux, usually neglected for the case of low salinity gradients, considerably reduce the RED unit exergy performance when high salinity gradients are applied.

The effect of varying saline solution concentrations (0.5-5 M for concentrate and 0.01-1 M for dilute) were investigated including high concentrated cases which required a more complex formulation of the model than those reported so far in the literature [43]. Also, the effect of operating conditions (e.g. external load, residence time and flow-arrangements) on exergy efficiency was investigated. Optimal operating conditions in order to achieve minimum exergy consumption and maximum process efficiency were identified for RED process in closed loop applications. In fact, in closed-loop applications exergy consumption related to the RED unit has to be restored by a thermal regeneration unit using low-grade waste heat. The higher the exergy destruction in the RED unit, the higher the thermal power required in the regeneration unit.

2 DESCRIPTION OF THE MODELLING APPROACH

The model, implemented in the software *Engineer Equation Solver* (EES) [44], is divided in three sub-sections:

(i) *Thermodynamics* section, which reports the model and equations used to describe the properties of electrolyte solutions (e.g. osmotic and activity coefficients, density and conductivity of NaCl solutions).

(ii) *1-D RED model* section, which describes the main phenomena involved in the process (e.g. electrical phenomena, mass balances, salt and water fluxes, etc.). Also, model validation is reported in this section.

(iii) *Exergy analysis* section, which predicts all the exergy fluxes on the basis of the 1-D RED model inputs and outputs.

2.1 Thermodynamics of electrolyte solutions

Modelling RED and exergy analysis require an accurate evaluation of thermodynamic properties of the solutions involved in the process. In particular, in this work, only NaCl solutions were considered but similar considerations can be easily applied for different electrolyte solutions.

As it is well known, the chemical potential of the generic solute *MX* of an electrolyte solution is defined in Eq. (1) [45].

$$\mu_{MX} = \mu_{MX}^{0} + \nu RT \ln\left(m_{\pm}\gamma_{\pm}\right) \tag{1}$$

In which $\mu°_{MX}$ is the chemical potential of the solute in the standard state (i.e., ideal 1 molal solution at 25°C and 1 atm), obtained as combination of the standard chemical potentials of the single ions, ν is the sum of ions in one molecule of solute ($\nu = \nu_{+} + \nu_{-}$), $m_{\pm}$ the mean molality and $\gamma_{\pm}$ the mean activity coefficient. The mean molality and activity coefficient are defined as geometric mean of the ions properties [45].

Similarly, the chemical potential of the solvent (i.e. water) is defined in Eq. (2).

$$\mu_{s} = \mu_{s}^{0} + RT \ln\left(a_{s}\right) \tag{2}$$

in which a_s is the solvent activity and $\mu_i°$ is the solvent chemical potential in the standard state.

The activity of the solvent is related to the osmotic coefficient ϕ, defined in Eq. 3.

$$\varphi = -\frac{1000 \ln(a_s)}{M_w \sum_i \nu_i m_i} \tag{3}$$

where M_W is the molecular weight of the solvent (g/mol), m_i is the i-ion molality in the solution (mol/kg), v_i the dissolution stoichiometric coefficient of i-ion.

2.1.1 *Osmotic and mean activity coefficients*

Pitzer's ion interaction model [45] is widely used to describe the behaviour of electrolyte solutions. In Pitzer's model, the osmotic and salt activity coefficients are described by semi-empirical equations in which the interactions of all ions in solution is taken into account by means of concentration-independent interaction coefficients. Thus, for an arbitrary composition of an aqueous electrolyte mixture, when the interaction coefficients are known, activities and osmotic coefficients of all ions can be estimated using Pitzer's model.

For the case of a generic electrolyte *MX*, the Pitzer's equations for osmotic and activity coefficients are reported in Eqs 4-6.

$$\varphi = 1 - |z_M z_X| A_\varphi \frac{I^{0.5}}{1 + bI^{0.5}} + 2m \frac{\nu_M \nu_X}{\nu} B^{\varphi}_{MX} + 2m^2 \frac{(\nu_M \nu_X)^{3/2}}{\nu} C^{\varphi}_{MX} \tag{4}$$

$$\ln(\gamma_\pm) = -|z_M z_X| A_\varphi \left(\frac{I^{0.5}}{1 + bI^{0.5}} + \frac{2}{b} \ln(1 + bI^{0.5}) \right) + 2m \frac{\nu_M \nu_X}{\nu} B^{\gamma}_{MX} + 3m^2 \frac{(\nu_M \nu_X)^{3/2}}{\nu} C^{\varphi}_{MX} \tag{5}$$

with

$$B^{\varphi}_{MX} = B^{(o)}_{MX} + B^{(1)}_{MX} \exp(-\alpha I^{0.5}) \tag{6.a}$$

$$B^{\gamma}_{MX} = 2B^{(o)}_{MX} + \frac{2B^{(1)}_{MX}}{\alpha^2 I} \left[1 - (1 + \alpha I^{0.5} - \frac{\alpha^2 I}{2}) \exp(-\alpha I^{0.5}) \right] \tag{6.b}$$

in which $m_0 = 1$ mol · kg^{-1} is the standard molality, $b = 1.2$ kg$^{1/2}$mol$^{-1/2}$ is a universal parameter; α is a numerical constant equal to 2 for univalent ions; I is the ionic strength A_ϕ,

is the Debye-Huckel parameter for the osmotic coefficient; z_M and z_X are the charges of cation and anion; $B^{(0)}_{MX}$, $B^{(1)}_{MX}$, and C_{MX} are adjustable parameters, called *ion-interaction parameters or virial coefficients*, related to short-range interaction between the ions, thus particularly

important when salt concentration is high. The virial coefficients are function of the electrolyte type, temperature and pressure. For some salts, like *NaCl* and *KCl* [46,47] some correlations to evaluate the interactions parameters were found in literature as function of temperature and pressure. Fig. 1 shows the dependence of osmotic and salt activity coefficients on concentration at 298 K.

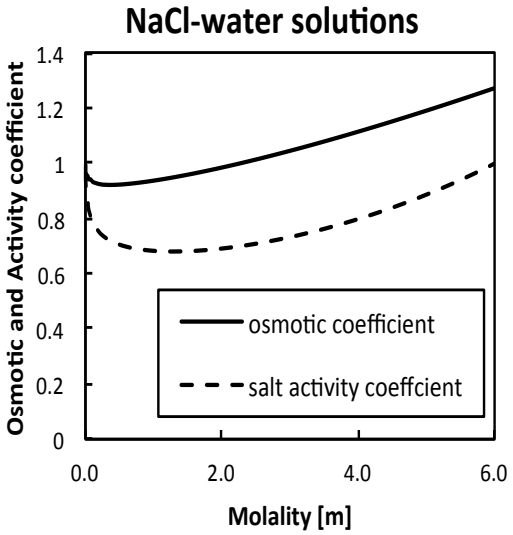

Fig. 1. Osmotic and salt activity coefficients for NaCl solution at 298.15 K as function of molality.

2.1.2 *Density*

The solutions density is also affected by salt concentration. For NaCl-water solutions, density was estimated as a linear function of the molar concentration according to Eq. 7.

$$\rho = \rho_0 + \left(\frac{\Delta\rho}{\Delta C}\right) \mathrm{C} \tag{7}$$

where ρ_0 is density of pure water at 298.15 K, which is equal to 997 kg/m^3. The slope of the function ($\Delta\rho/\Delta C$) was evaluated by fitting experimental data from literature [48]. For NaCl $\Delta\rho/\Delta C$ is equal to 37.4 kg/mol. Fig. 2.a shows the density of NaCl aqueous solution as function of the molar concentration.

2.1.3 *Conductivity*

Solutions conductivity is another important property to be estimated, as it affects the electrical resistance of the solutions within the stack. Solutions with very low electrolyte concentration

exhibit very low conductivity and high electrical resistance. The dependence of solution equivalent electrical conductivity on concentration was estimated according to Eq. 8.

$$\Lambda = \Lambda_0 - \frac{A_\Lambda C^{1/2}}{1 + B_\Lambda C^{1/2}} - C_\Lambda C \tag{8}$$

where Λ_0 is the equivalent conductivity of salt at infinite dilution, A_Λ, B_Λ and C_Λ are fitting parameters, and C is the molar concentration. The parameters for NaCl solutions were obtained fitting literature experimental results [48]. At 298 K, A_Λ=*91.02*, B_Λ=*1.66* and C_Λ=*6.80.* Fig. 2.b shows the conductivity of NaCl solution as function of the solution molar concentration.

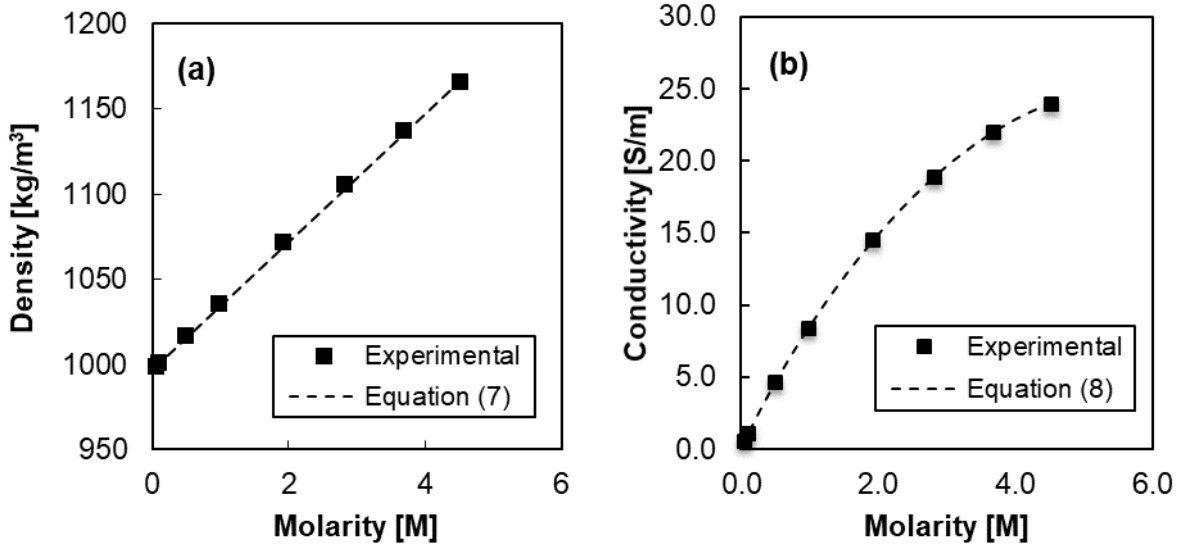

Fig. 2. Comparison between experimental [48] and fitting results of density (a) and conductivity (b) of NaCl solutions versus molarity at 298.15 K.

2.2 RED process modelling

A schematic representation of a generic RED unit is reported in Fig. 3 along with the indication of the repetitive unit, here named *cell pair*. A cell pair consists of two channels, in which the two solutions at different concentration (the dilute and the concentrate) flow, an anionic and a cationic exchange membrane.

In agreement with previous studies available in the literature [40], [49], the present model is based on a few simplifying assumptions:

- a mono-dimensional approach was used to describe the system, considering the variation of the main variables (concentrations, electrical current, fluxes, resistances etc.) along the channel length (L) coinciding with the flow direction (both in co- and counter-current arrangement);
- salt concentration profiles (along the direction perpendicular to the IEMs) are assumed to be flat in both compartments, i.e. concentration polarisation phenomena are neglected;
- all cell pairs operate in the same way, assuming an ideal flow distribution with no parasitic currents [50].

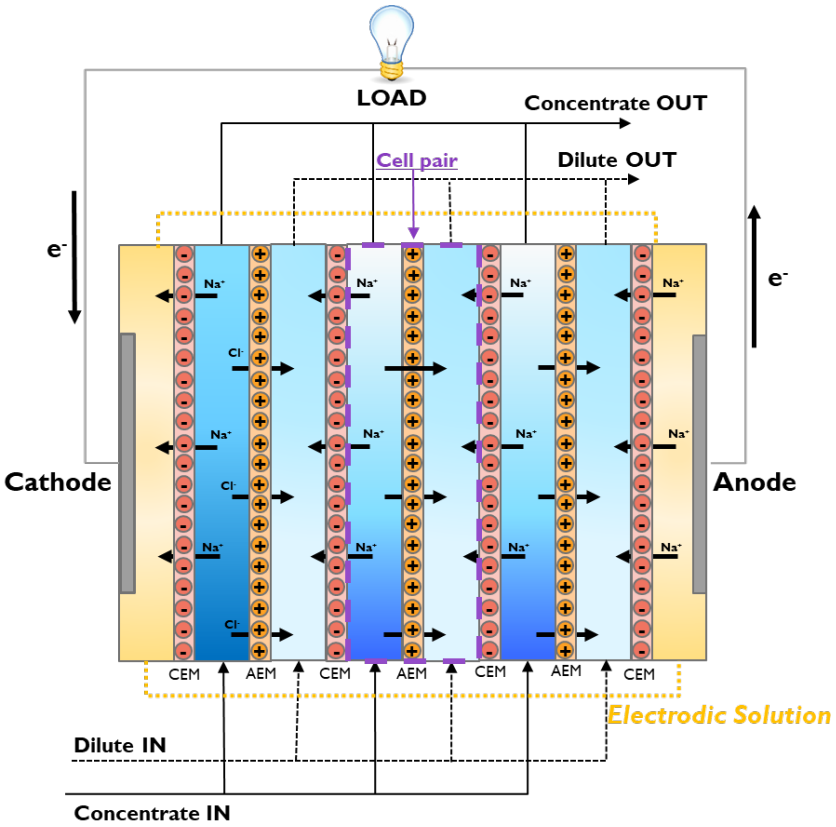

Fig. 3. Schematic representation of a RED unit.

In addition, given the preliminary nature of the present work, no pressure drop along the channel was considered and gross power values only are reported. In fact, pressure drops are strongly related to stack geometry and configuration, and the present analysis does not consider these aspects of the unit design. However, several works reported in literature provide useful

information on how pressure drops are affected by stack geometry by means of theoretical [51,52] or experimental investigations [53,54].

The equivalent circuit scheme of the RED unit is reported in Fig. 4.a. The stack can be imagined as consisting of N_k parallel branches where N_k is the number of intervals adopted for the numerical discretization of the domain along the flow direction (channel length). Each of them supplies part of the current I circulating in the external circuit and consists of N_{cp} (cell pair number) identical repetitive units connected in series. As shown in Fig. 4.b, each cell pair is divided in N_k elements of length Δx along the main flow direction ($\Delta x = L/N_k$). The generic k-th element is constituted of two electric voltage generators, one for each IEM (E_{CEM} and E_{AEM}), and four resistances, relevant to the solutions (R_{conc} and R_{dil}) and the IEMs (R_{CEM} and R_{AEM}) resistances. It is worth noting that the sketch in Fig. 4.b is only a schematic representation of the phenomena involved in the cell pair. Finally, RED equivalent circuit of Fig. 4.a is serially connected to a branch indicating the resistance of the electrodic compartments R_{blank} and, eventually, closed by the external load resistance R_L.

All the variables presented in this scheme will be described in details in the following paragraphs.

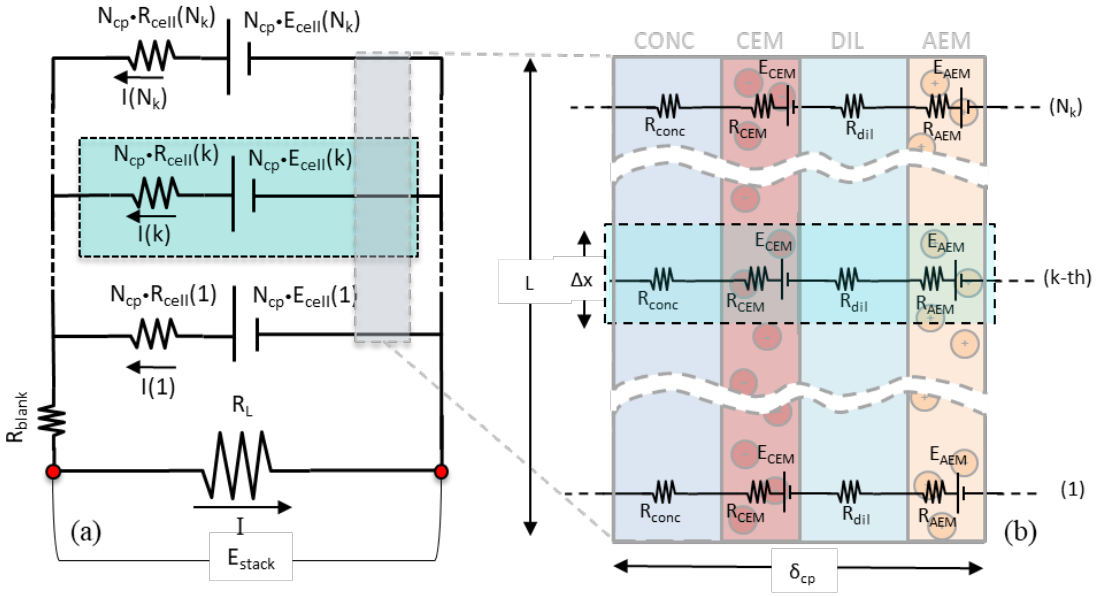

Fig. 4. Equivalent electrical circuit scheme of the RED unit (a) and of an individual cell pair (b).

The voltage generated from each kth element of cell pair (E_{cell}), is calculated by an equation formally similar to the Nernst equation (Eq. 9).

$$E_{cell}(k) = E_{CEM}(k) + E_{AEM}(k) = 2\alpha_{av}(k)\frac{RT}{F}\ln\left(\frac{m_{conc}(k)\cdot\gamma_{conc}(k)}{m_{dil}(k)\cdot\gamma_{dil}(k)}\right) \quad (9)$$

in which α_{av} is the average permselectivity of the two IEMs. The kth internal resistance is made of 4 series resistances as reported in Eq. 10.

$$R_{cell}(k) = \left[R_{CONC}(k) + R_{DIL}(k) + R_{CEM}(k) + R_{AEM}(k)\right]\cdot\frac{1}{\Delta x\cdot b} \quad (10)$$

where $R_{conc}(k)$ and $R_{dil}(k)$ are the electrical resistances of feed compartments, while $R_{CEM}(k)$ and $R_{AEM}(k)$ are the IEMs resistances. The feed compartments resistance is calculated according to Eq. 11.

$$R_{sol}(k) = f\frac{\delta_{sol}}{\Lambda_{sol}(i)\cdot C_{sol}(k)} \quad (11)$$

where f is called obstruction factor and represents a correction term which takes into account the increase of electrical resistance caused by the presence of the spacer (e.g. due to tortuosity of ion path or shadow effect on membranes). The value of the obstruction factor is reported in Table 2. The subscript sol indicates either the concentrate or dilute compartment.

The electric current (i) generated in each ith branch of the circuit is calculated from equation 12.a:

$$E_{cell}(k) = i(k)R_{cell}(k) + E_{stack} + R_{blank}I \quad (12.a)$$

which can be rearranged into equation 12.b:

$$i(k) = \frac{E_{cell}(k) - (E_{stack} + R_{blank}I)}{R_{cell}(k)} \quad (12.b)$$

where E_{stack} is the stack voltage, the electric potential measurable from the outside of the RED unit and R_{blank} is the resistance of the electrodic compartments. The electric current circulating

on the external load is the sum of each one produced in the "k-th" branch (*Kirchhoff's junction rule*).

$$I = \sum_k i(k) \tag{13}$$

The closing equation is obtained by the ohm-law on the external load (Eq. 14).

$$E_{stack} = R_L \cdot I \tag{14}$$

The Gross power (P_{RED}) and gross power density (P_d) of the RED unit are calculated according to Eq. 15.a and Eq.15.b.

$$P_{RED} = N_{cp} \cdot E_{stack} \cdot I \tag{15.a}$$

$$P_d = \frac{P}{N_{cp} \cdot A_{cp}} \tag{15.b}$$

where A_{cp} is the membrane area of a cell pair.

The ohmic loss due to the internal resistance of the RED unit is calculated according to Eq. 16.

$$P_{loss} = \sum_k R_{cell}(k) \cdot I(k)^2 + r_{blank} I^2 \tag{16}$$

2.2.1 *Water and salt flux through the IEMs*

The salinity gradient across each membrane is responsible also of some detrimental effects producing uncontrolled mixing phenomena, which reduce the driving force of the process, generally identified with water flux (J_w) and salt flux (J_s). In Fig. 5 a schematic representation of fluxes across the IEMs is provided.

Due to non-ideality of the membranes ($\alpha_{av} \neq 1$) few co-ions pass through the IEMs resulting in a diffusive flux of salt. The total salt flux from the two contiguous concentrate channels to the dilute one is described by Eq. 17.

$$J_s(k) = J_{mig}(k) + J_{diff}(k) = \frac{i(k)}{zF} + 2\frac{P_s}{\delta_m}\left[C_{CONC}(k) - C_{DIL}(k)\right] \tag{17}$$

where i is the current density or the current for unit of membrane area, δ_m is membrane thickness (assumed equal for both IEMs and value reported in Table 2.) and P_s is the salt permeability (value reported in Table 2.). Using the same approach adopted in [55], the permeability (P_s) is the product of salt diffusion and sorption coefficient in membrane.

In Eq. 17, the first term, the *migrative flux* (J_{mig}), gives the salt transferred with the counter-ions migration through the AEM and the CEM, while, the second term, the *diffusive flux* (J_s), refers to the salt flux due to the co-ions diffusion. Factor 2 multiplying the second term takes into account the presence of two IEMs in contact with the dilute channel.

Also the water flux consists of two terms (Eq. 18): (i) the first named *osmotic flux,* generated by the osmotic pressure difference between the two solutions and directed from the dilute to the concentrate chamber; (ii) the second named *electro-osmotic flux,* due to the water molecules transported in the solvation shell of the ions and directed in opposite direction.

$$J_w(k) = J_{osm}(k) + J_{eosm}(k) = -2\ \nu\ RTP_w\left[C_{CONC}(k)\phi_{CONC}(k) - C_{DIL}(k)\phi_{DIL}(k)\right] + n \cdot J_s(k) \qquad (18)$$

where P_w is the average water permeability of the IEMs (value reported in Table 2), ϕ the osmotic coefficient and n the hydration number for Na^+ and Cl^-. The hydration number was fixed equal to 7 according to [49]. From Eq. 18 a volumetric water flux is calculated (m/s).

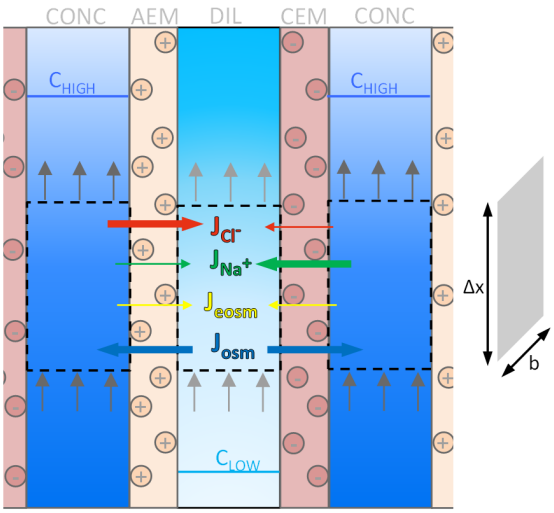

Fig. 5. Schematic representation of the modelled fluxes across the IEMs.

2.2.2 *Salt and Global Mass Balances*

For each computational domain element, considering a co-current flow arrangement, salt mass balance and global mass balance equations in each compartment (dilute and concentrate) are applied to calculate the exiting concentration and flow rate. These are adopted as inlet conditions of the following element, thus solving the system of equations and characterizing concentration and flow-rate profiles along the entire channel length.

In particular, for the concentrate channel, equations 19 and 20 can be written:

$$C_{conc}(k+1)Q_{conc}(k+1) = C_{conc}(k)\cdot Q_{conc}(k) - J_s(k)b\Delta x \tag{19}$$

$$\rho_{conc}(k+1)\cdot Q_{conc}(k+1) = \rho_{conc}(k)\cdot Q_{conc}(k) - J_w(k)\cdot b\Delta x\frac{\rho_w}{M_w} - J_s(k)\cdot b\Delta x M_s \tag{20}$$

where $C_{conc}(k+1)\cdot Q_{conc}(k+1) = C_{conc,out}(k)\cdot Q_{conc,out}(k)$ is the product of outlet concentration and flow-rate of the exiting concentrate solution (i.e. the salt molar flow rate), while $C_{conc}(k)\cdot Q_{conc}(k) = C_{conc,in}(k)\cdot Q_{conc,in}(k)$ is the product of concentration and flow-rate of the concentrate inlet solution.

In a similar way, for the dilute channel, equations 21 and 22 are obtained:

$$C_{dil}(k+1)Q_{dil}(k+1) = C_{dil}(k)\cdot Q_{dil}(k) + J_s(k)b\Delta x \tag{21}$$

$$\rho_{dil}(k+1)\cdot Q_{dil}(k+1) = \rho_{dil}(k)\cdot Q_{dil}(k) + J_w(k)\cdot b\Delta x\rho_w + J_s(k)\cdot b\Delta x M_s \tag{22}$$

When a counter-current arrangement is considered, the mass balances are formally the same, though the inlet-outlet flow-rate terms in the dilute channel mass balance have the opposite sign, as shown in Eqs 21.a and 22.b.

$$C_{dil}(k)Q_{dil}(k) = C_{dil}(k+1)\cdot Q_{dil}(k+1) + J_s(k)b\Delta x \tag{21.a}$$

$$\rho_{dil}(k)\cdot Q_{dil}(k) = \rho_{dil}(k+1)\cdot Q_{dil}(k+1) + J_w(k)\cdot b\Delta x\rho_w + J_s(k)\cdot b\Delta x M_s \tag{22.b}$$

where $C_{dil}(k+1)\cdot Q_{dil}(k+1) = C_{dil,in}(k)\cdot Q_{dil,in}(k)$ is the product of dilute inlet concentration and dilute inlet flow-rate, while $C_{dil}(k)\cdot Q_{dil}(k) = C_{dil,out}(k)\cdot Q_{dil,out}(k)$, is the product of dilute outlet concentration and flow-rate.

The solution flow-rates feed to the pile were selected imposing an inlet velocity of 1 cm/s within the channel, typical values adopted in RED systems [56].

2.2.3 *Membranes properties for NaCl solutions*

The IEMs behaviour is characterized by means of several properties already presented in the previous sections. The most relevant properties are the *permselectivity* (α_{AEM} or α_{CEM}), which identifies the selectivity of membrane to the passage of counter ions and rejections of co-ions, and *electrical resistance* (R_{AEM} or R_{CEM}). Other important features are the *water* and *salt permeability* (P_w and P_s), which generate the osmotic water flux and diffusive salt flux, respectively. Manufacturers usually provide the values of these properties in reference conditions. In this work, Fujifilm's membranes were considered. Constant values of water and salt permeability, were fixed (see Table 2), while concentration dependent correlations were evaluated both permselectivity and electric resistance.

2.2.4 *Numerical details*

The integrated model was implemented in *Engineer Equation Solver* (EES) using the Euler's method to solve the mass balance equations. In this method, the numerical accuracy of the solution depends on the discretization length (Δx), which is a function of N_k and L. In order to identify the N_k value which gives a good compromise in accuracy and time calculation, a grid dependence analysis was performed, considering the longest RED unit presented in this study (L=1.0 m, b=0.1 m). As shown in Fig. 6, the grid dependence analysis indicates that a discretization length of 2.5 cm (40 steps) is small enough to get stable and accurate solutions. Further, passing from 40 to 50 discretization intervals the power output varies less than 1% and concentration profiles are practically overlapped.

Table 2. Physical and geometrical parameters assigned for simulations

Parameter		Value
P_w [1]	[m/(Pa·s)]	$2.22 \cdot 10^{-14}$
δ_m	[m]	$1.25 \cdot 10^{-4}$
P_s	[m^2/s]	$1 \cdot 10^{-12}$
α_{av} [2]	[%]	95-98
$R_{AEM}=R_{CEM}$ [3]	[ohm cm^2]	1.5
f	[-]	1.5625

[1] *experimental values measured @ ref. conditions: T=25°C, C_{conc}=3 M C_{dil}=0.05M.*
[2] *experimental values measured @ ref. conditions: T=25°C, C_{conc}=0.5M C_{dil}=0.05M.*
[3] *experimental values measured @ ref. conditions: T=25°C, C_{sol}=2 M.*

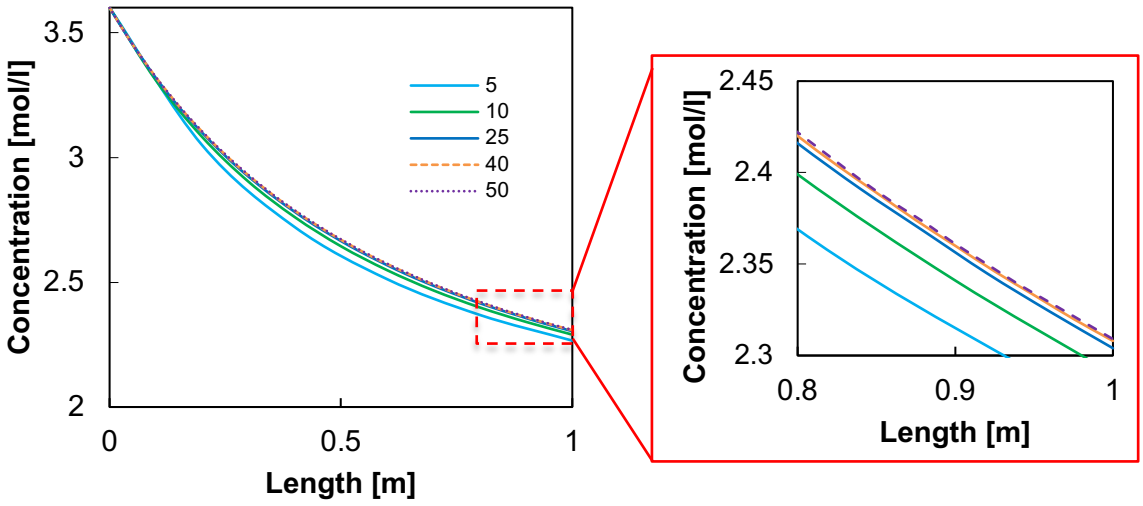

Fig. 6. Grid dependence analysis: concentration profiles along the channel varying the number of grid elements (N_k). RED stack of 1000 cell pairs 0.1 m x 1.0 m, $v_{conc}=v_{dil}$=1 cm·s^{-1}, C_{conc}=3.6 M C_{dil}=0.05 M.

2.2.5 *Model validation*

The mono-dimensional RED model was validated by comparison with experimental results reported in the literature [57]. Fig. 7.a and 7.b show the trend of experimental stack voltages and power densities for three different concentrate concentrations (i.e. 0.5, 2 and 5 M) as function of the current and the stack voltage, respectively.

Model predictions fit very well experimental trends, thus indicating the reliability of the model in the investigated concentration range. Model was further validated with different flow velocities and stack dimensions, resulting always in a good agreement between predictions and experiments. However, relevant graphs are omitted for the sake of brevity.

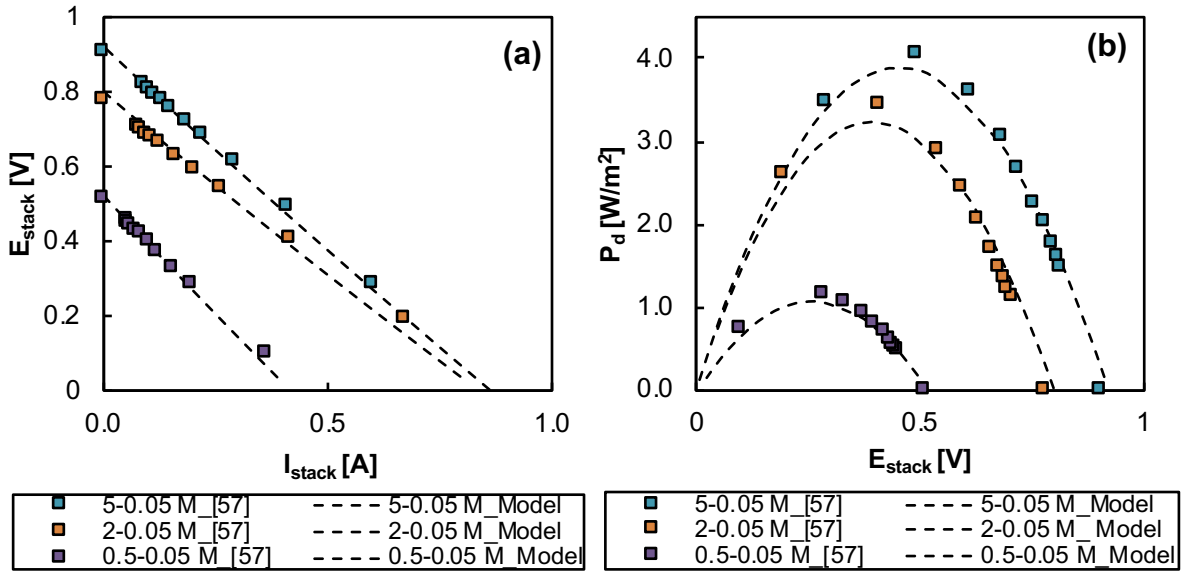

Fig. 7. Comparison between experimental trends and model predictions for (a) stack potential and (b) power density [57] . Operating conditions: 5 cell pairs-stack, A=0.1×0.1m^2; C_{dil}=0.05 M; C_{conc}=0.5 M, 2 M, 5 M; v_{dil}=v_{conc}=2 cm/s, T=25°C.

2.3 Exergy Analysis

Eq. 23 presents the general formula used for calculating the exergy of a stream flow at pressure p, temperature T and composition x_i (where the subscript "i" refers to species "ith" compounding the mixture)[58].

$$\dot{B} = \sum_{i=1}^{n} \left[\left(\tilde{h}_i(T,p,x_i) - T_0 \tilde{s}_i(T,p,x_i) \right) - \left(\tilde{h}_i(T_0,p_0,x_{i,0}) - T_0 \tilde{s}_i(T_0,p_0,x_{i,0}) \right)_0 \right] \dot{N}_{i,in} \qquad (23)$$

$\tilde{h}_i$ and $\tilde{s}_i$ are respectively the partial molar enthalpy and entropy of the "ith" species compounding the mixture function of T, p, x_i; the subscript "0" refers to equilibrium conditions with the environment.

According to the well-known approach proposed by Szargut [59], in order to assess whether (and how much) work is produced by a change in chemical composition or by changes in temperature and pressure of the stream, exergy is commonly split into two fractions:

- *Physical exergy*: this fraction is the amount of work obtained when the stream reaches reversibly thermal and mechanical equilibrium with the environment, while not

changing its chemical composition. The thermodynamic state reached by the system is characterized by the same temperature and pressure of the environment, and it is commonly named "*restricted dead state*";

- *Chemical exergy*: this fraction indicates the amount of work obtained when the stream reaches chemical equilibrium with the environment, while keeping its temperature and pressure equal to T_0 and p_0. The thermodynamic state of the system in equilibrium with the environment is commonly indicated as "*dead state"*.

Eq. 24 and 25 express physical and chemical exergy respectively.

$$\dot{B}_{ph} = \sum_{i=1}^{n} \left[\left(\tilde{h}_i \left(T, p, x_i \right) - T_0 \tilde{s}_i \left(T, p, x_i \right) \right) - \left(\tilde{h}_i \left(T_0, p_0, x_i \right) - T_0 \tilde{s}_i \left(T_0, p_0, x_i \right) \right) \right] \cdot \dot{N}_{i,in} \tag{24}$$

$$\dot{B}_{ch} = \sum_{i=1}^{n} \left[\left(\tilde{h}_i \left(T_0, p_0, x_i \right) - T_0 \tilde{s}_i \left(T_0, p_0, x_i \right) \right) - \left(\tilde{h}_i \left(T_0, p_0, x_{i,0} \right) - T_0 \tilde{s}_i \left(T_0, p_0, x_{i,0} \right) \right) \right] \cdot \dot{N}_{i,in} =$$

$$= \sum_{i=1}^{n} \left[\mu_i \left(T_0, p_0, x_i \right) - \mu_i \left(T_0, p_0, x_{i,0} \right) \right] \cdot \dot{N}_{i,in} \tag{25}$$

Differently from energy which can be neither created nor destroyed, exergy is always consumed due to irreversible phenomena which naturally occur in real processes. Some example of sources of irreversibility are flow friction, uncontrolled mixing phenomena and heat transfer through finite temperature difference. By applying an exergy balance, it is possible to assess the amount of exergy destroyed (*Ir)* due to irreversibility.

$$\sum_{j \in Input} \dot{B}_j - \sum_{h \in Output} \dot{B}_h = \dot{I}r \tag{26}$$

As previously explained, in RED process, electric power is generated by ions transfer between two solutions at different concentration. Since chemical composition of both streams changes when passing through a RED unit, part of their chemical exergy is used to generate electricity. Only in the case of reversible operation of a RED unit, the overall exergy variation would be entirely converted into electrical power.

In order to assess the magnitude of exergy destruction occurring within RED unit, an exergy balance is set out as shown in Eq. 27. The variation of the chemical exergy of dilute and concentrate solutions is described on the LHS, while the electrical power produced P_{RED} and the exergy destroyed due to irreversibility $Ir_{,RED}$ appear on the RHS.

$$\left(\dot{B}_{conc,in}-\dot{B}_{conc,out}\right)+\left(\dot{B}_{dil,in}-\dot{B}_{dil,out}\right)=\dot{P}_{RED}+\dot{I}r_{RED} \tag{27}$$

Since a RED unit often operates at environmental temperature (i.e. approximately T_0= 298 K) and pressure (i.e. approximately p_0=100 kPa), only chemical exergy was considered throughout the analysis, neglecting physical exergy variations within the unit. As already mentioned, no pressure drops were considered in the model, thus pressure was considered constant along the channels. Seawater composition of 38000 ppm NaCl was considered as reference state to evaluate the chemical exergy of each stream.

Eqs 28 and 29 provide the chemical exergy variation of concentrate and dilute solutions respectively. Both equations were derived from Eq. 25 where chemical potential are explicitly expressed in terms of activities of salt and water, calculated by means of Eqs 1-6.

$$\dot{B}_{conc,in}-\dot{B}_{conc,out}=$$

$$=RT_0\left[\dot{N}_{conc,in}\left(x_{s,conc}^{in}\,v\ln\left(\frac{a_{s,conc}^{in}}{a_{s,0}}\right)+x_{w,conc}^{in}\ln\left(\frac{a_{w,conc}^{in}}{a_{w,0}}\right)\right)-\dot{N}_{conc,out}\left(x_{s,conc}^{out}\,v\ln\left(\frac{a_{s,conc}^{out}}{a_{s,0}}\right)+x_{w,conc}^{out}\ln\left(\frac{a_{w,conc}^{out}}{a_{w,0}}\right)\right)\right] \tag{28}$$

$$\dot{B}_{dil,in}-\dot{B}_{dil,out}=RT_0\left[\dot{N}_{dil,in}\left(x_{s,dil}^{in}\,v\ln\left(\frac{a_{s,dil}^{in}}{a_{s,0}}\right)+x_{w,dil}^{in}\ln\left(\frac{a_{w,dil}^{in}}{a_{w,0}}\right)\right)-\dot{N}_{dil,out}\left(x_{s,dil}^{out}\,v\ln\left(\frac{a_{s,dil}^{out}}{a_{s,0}}\right)+x_{w,dil}^{out}\ln\left(\frac{a_{w,dil}^{out}}{a_{w,0}}\right)\right)\right] \tag{29}$$

Exergy efficiency can be defined as the ratio of electric power produced to the variation of chemical exergy of dilute and concentrate solutions.

$$\eta_{ex}=\frac{\dot{P}_{RED}}{\left(\dot{B}_{conc,in}-\dot{B}_{conc,out}\right)+\left(\dot{B}_{dil,in}-\dot{B}_{dil,out}\right)} \tag{30}$$

Exergy efficiency indicates the percentage of the chemical exergy consumed within RED stack which is usefully converted into electrical power. As it will be shown in the next section, it

represents a useful thermodynamic indicator whose numerical values provide insights on the effect of irreversibility for alternative design and operating scenarios of RED process.

3 RESULTS AND DISCUSSION

The integrated model was used to perform several sensitivity analyses in order to investigate the effects of irreversibility sources (permselectivity, water and salt fluxes, all linked to the membrane properties), flow arrangements (co and counter current) and residence times on the exergy efficiency of the process. A stack of 1000 cell pairs was considered in order to neglect the effect of the electrodic compartment resistance (R_{blank}) on RED performance.

3.1 Effect of the irreversibility source

Exergy analysis of RED unit was carried out considering a stack equipped with square membranes of 0.1 m x 0.1 m. As regards concentrate and dilute feeds, *NaCl* solutions with a concentration respectively of 3.6 M and 0.05 M were supplied to the RED unit. The inlet velocity of both streams was set equal to 1 cm/s. The main sources of irreversibility involved in RED process are: (i) *internal ohmic losses* (P_{loss}), which identify the power dissipated by the internal resistances (Eq. 16); (ii) *membrane permselectivity* (α), which affects the electro-motive force of the pile (Eq. 9); (iii) *diffusive salt flux* (J_s), which identifies the co-ions transport across the IEM (Eq. 17); *water flux* (J_w), which identifies the flux of water across the IEM (Eq. 18).

In order to assess at which extent each irreversibility source affects the exergy performance of the unit, four different scenarios were considered:

- *Scenario A:* the pile is equipped with ideal membranes (P_w=0 m/(Pa·s), P_s=0 m^2/s and α=1) and internal resistance of the pile is considered as unique source of irreversibility;
- *Scenario B*: the effect of non-ideal permselectivity on the Donnan potential generation at the IEMs-solutions interface (and consequentially, on the electro-motive force) is

considered still neglecting diffusive water and salt fluxes in the transport equations (P_w=0 m/ (Pa·s), P_s=0 m^2/s and $\alpha \neq 1$);

- *Scenario C:* non-ideal permselectivity and diffusive salt flux (P_s=10^{-12} m^2/s and $\alpha \neq 1$), conversely, diffusive water flux is neglected (P_w=0 m/ (Pa·s));
- *Scenario D:* the pile is equipped with real membranes all the irreversibility sources are considered (P_w=2.22·10^{-14} m/ (Pa·s), P_s=10^{-12} m^2/s and $\alpha \neq 1$).

In Fig. 8.a and b, the exergy efficiency and power density are shown for each simulated scenario as a function of the ratio between external load and internal stack resistance (R_L/R_{int}). More specifically, when considering R_L/R_{int} equal to 0, the stack operates in short-circuit condition (SC): in this case the maximum electrical current through the pile is observed and no electrical power is produced. Conversely, when R_L/R_{int} tend to ∞, the pile works in open circuit condition (OC): in this case, the stack voltage is equal to the electro-motive force and no electric current circulates in the system. As shown in Fig. 8.b, the maximum power density is obtained when the ratio R_L/R_{int} is approximately 1, with stack voltage equal to half of the Open Circuit Voltage [60].

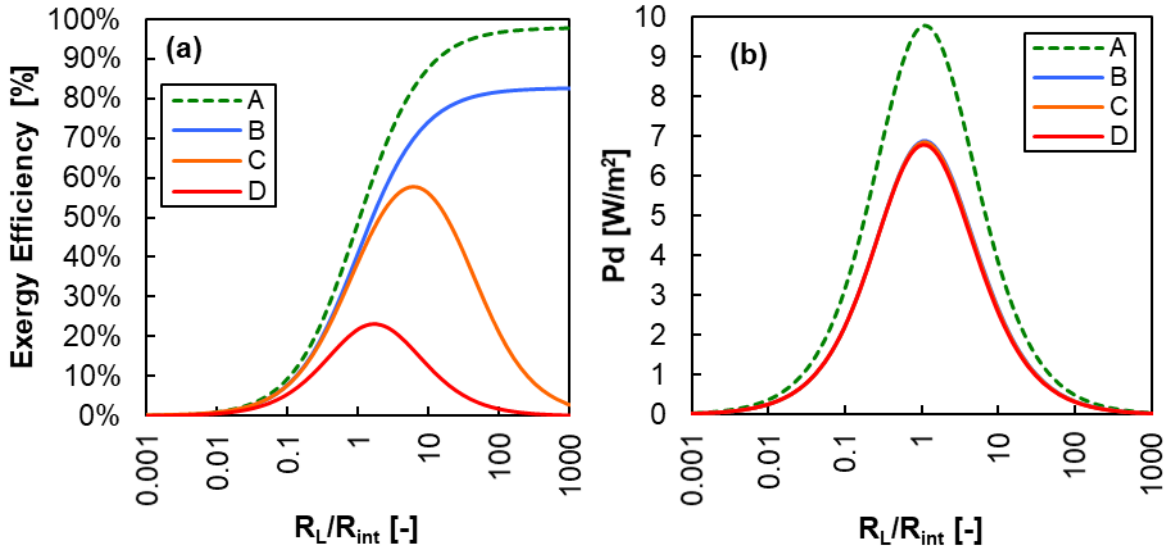

Fig. 8. Exergy Efficiency (a) and Power density (b) as a function of external/internal resistance ratio for each examined scenario. RED stack 0.1 m x 0.1 m, v_{conc}=v_{dil}=1 cm·s^{-1}, C_{conc}=3.6 M C_{dil}=0.05 M.

As shown in Fig. 8.a, when considering SC condition in all simulated scenarios, exergy efficiency is equal to zero, indicating that the exergy consumed is entirely destroyed by the pile internal resistance without producing electric power.

In *Scenario A*, RED exergy efficiency increases with the R_L/R_{int} ratio. It is worth noting that exergy efficiency is nearly equal to unity when approaching OC condition. This result indicates that under this circumstance, reversible transformation occurs within the pile, all the irreversibility approach to zero. When R_L/R_{int}=1, the exergy efficiency is equal to 0.5: half of the exergy consumption is converted into electric power by the pile, being the other fraction dissipated due to internal stack resistance.

In *Scenario B* the effect of non-ideal membrane permselectivity on the electrical voltage is taken into account. Comparing to case A, a similar trend for exergy efficiency is observed but lower values are obtained due to the decrease in the electro-motive force and power output (see eq. 9).

In both A and B scenarios maximum exergy efficiency is obtained in OC condition though the power output from the stack tends to zero. In this ideal condition solutions are virtually mixed through reversible steps with an infinitesimal current thus reducing to zero ohmic dissipations.

As previously mentioned, in case C salt diffusion and permselectivity were considered as sources of irreversibility, conversely, for case D, also osmosis was included. In these scenarios the exergy efficiency curve increases with the R_L/R_{int} ratio up to reach the maximum value slightly after the maximum power density (R_L/R_{int} between 1 and 10), while decreasing for higher values of R_L/R_{int}. In fact, a larger external load lowers the current (and the power output), while uncontrolled mixing phenomena keep the same absolute influence on mixing dissipation (as shown in Fig. 9.a) as they only depend on salinity gradient and salt/water permeability of IEMs. This leads to a dramatic increase of the relative effect of irreversible phenomena on exergy efficiency, so that, in OC conditions, exergy efficiency approaches zero: even with zero electric current exergy can be totally destroyed within the stack due to uncontrolled mixing phenomena.

For the case of a pile equipped with real membranes, Fig. 9 shows a breakdown of the exergy consumption (Ex_{cons}) into exergy destruction due to uncontrolled mixing phenomena ($E_{mix,}$), exergy destruction due to ohmic dissipation (P_{cons}), and electric power produced. It is interesting to observe how irreversibility magnitude due to uncontrolled mixing phenomena is almost equal for all operating conditions. Under these conditions, E_{mix} is dominated by the osmotic water transport, with migrative salt flux playing only a minor role in enhancing it when current is increased, contrarily to the effect of electro-osmosis (directly promoted by the current increase). Indeed, osmosis and salt diffusion phenomena themselves are indirectly reduced when current increase due to the reduction of concentration gradients. All these complex and counteracting phenomena lead to only a slight reduction (less than 5%) of $E_{mix,}$ observed when increasing stack current. Conversely, exergy destruction due to internal ohmic resistance strongly affects exergy performance when load resistance lower than internal stack resistance is considered, whereas being negligible when approaching OC condition.

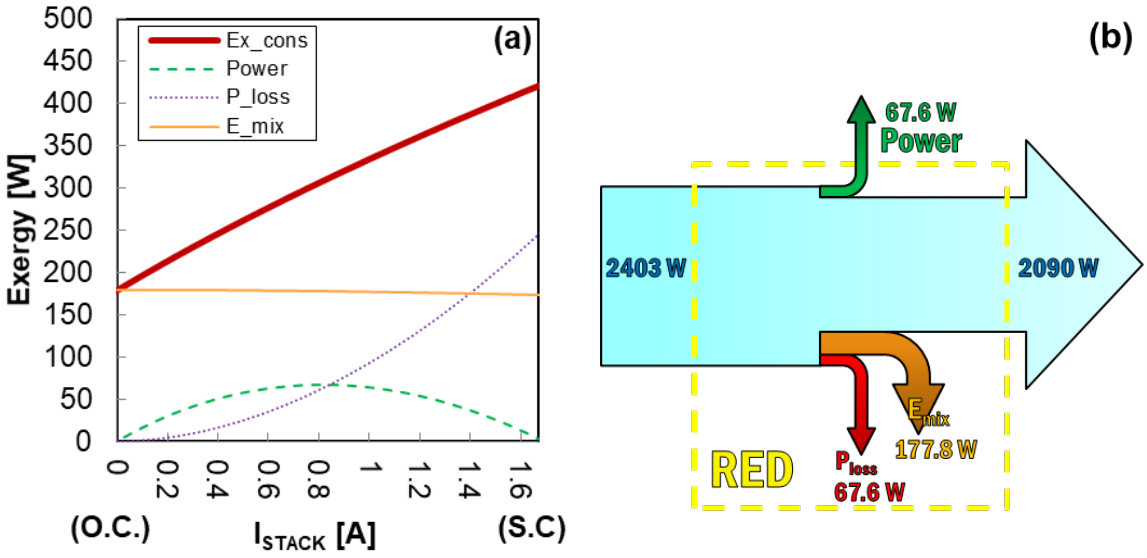

Fig. 9. (a) Variation of exergy consumption/conversion terms as a function of the electrical current (I) showing total consumed exergy (*Ex_cons*), power output (*Power*), ohmic losses (*P_loss*) and uncontrolled mixing phenomena (*E_mix*); (b) Graphical breakdown of exergy consumption/conversion terms for a real RED process in maximum power conditions. RED stack 0.1 m x 0.1 m, v_{conc}=v_{dil}=1 cm·s^{-1}, C_{conc}=3.6 M C_{dil}=0.05 M, scenario D.

3.2 Effect of membrane properties

In the previous analysis, fixed values of membrane salt and water permeability were considered. It is worth assessing how the RED exergy performance may change when equipping this membrane parameters change. To this aim, a sensitivity analysis changing salt and water permeability was carried out. Results are shown in Fig. 10. In particular:

- In Fig. 10.a, salt permeability P_s was fixed equal to $P_s=10^{-12}$ m^2/s, while water permeability P_w was varied in the range of $2.22\cdot10^{-14}$ to 0 m/(Pa·s). It can be observed how exergy efficiency improves from 23% to 58%, when water flux is null: this proves a strong impact of water flux on the unit performance.
- In Fig. 10.b, a similar analysis was carried out by considering a reduced salt permeability from 10^{-12} m^2/s to 10^{-11} m^2/s. Results show a strong reduction of exergy efficiency due to the increase of salt flux effect. In particular, when no osmosis is considered (i.e. $P_w = 0$), the exergy efficiency is reduced from 58% to 27%.

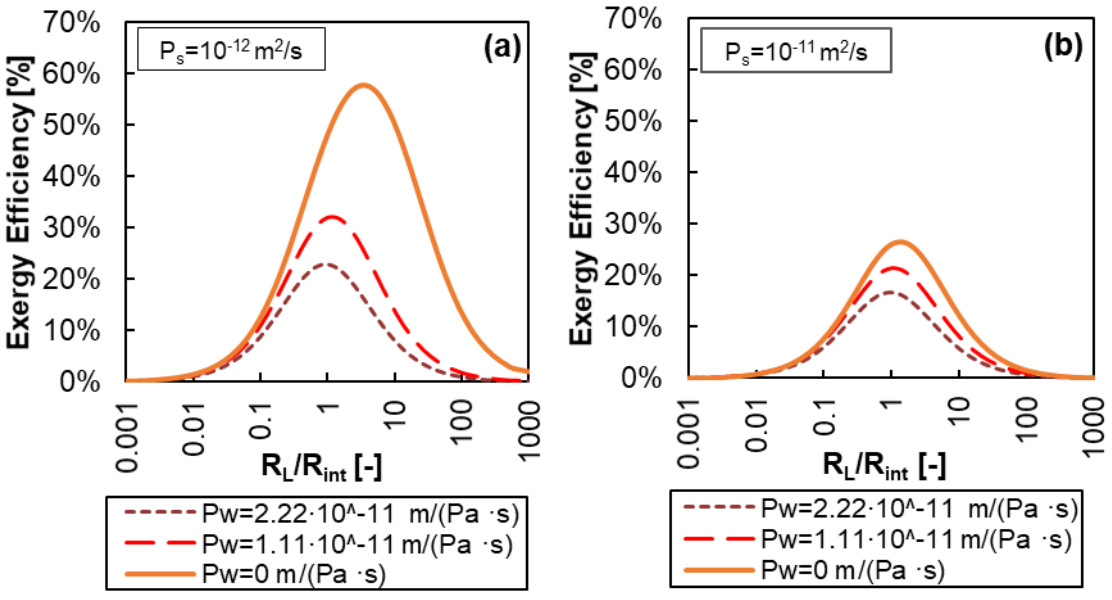

Fig. 10. Effect of diffusive water and salt flux on RED exergy efficiency varying the resistance ratio and assuming three different values for P_w ($2.22\cdot10^{-14}$, $1.11\cdot10^{-14}$ and 0 m/(Pa·s)) fixing P_s equal to 10^{-11} m^2/s in fig. (a) and 10^{-12} m^2/s in fig. (b). RED stack 0.1 m x 0.1 m, v_{conc}=v_{dil}=1 cm·s^{-1}, C_{conc}=3.6 M C_{dil}=0.05 M.

3.3 Effect of concentrate and dilute concentrations

In this section, the influence of inlet concentrations on the exergy efficiency and power density is analysed. As already mentioned, one of the main advantage of RED-HE is the possibility of selecting suitable feed concentrations which could lead to a more performing process.

For the analysis, the same stack configuration previously proposed was considered.

First, the effect of the concentrate was evaluated by gradually decreasing its concentration from 5.0 M to 0.5 M while keeping a dilute fixed to 0.05 M. Conversely, in the second analysis, the dilute concentration was increased from 0.05 M to 1 M while keeping a concentrate at 3.6 M.

Exergy efficiency and Power densities for all simulated cases are shown in Fig. 11.a-b and Fig. 12.a-b.

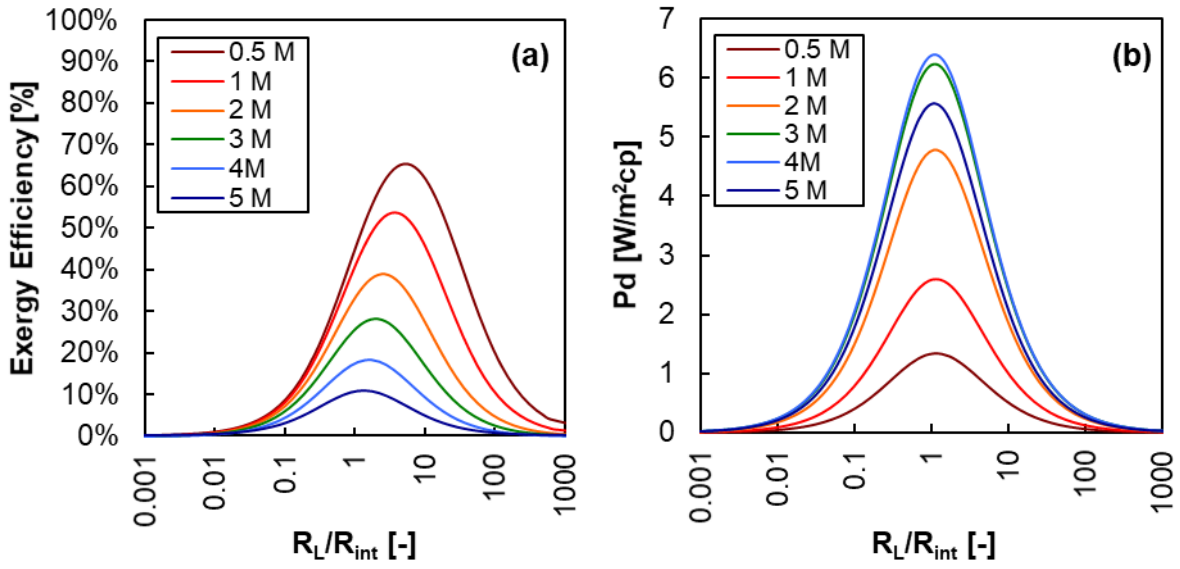

Fig. 11. Exergy efficiency (a) and Power density (b) as function of the R_L/R_{int} ratio and the concentrate solution concentration, setting the dilute concentration at 0.05 M. RED stack 0.1 m x 0.1 m, v_{conc}=v_{dil}=1 cm·s^{-1}, scenario D.

Results shown in Fig. 11.a-b indicate that a decrease in concentrate from 5.0 M to 0.5 M produces a substantial improvement of exergy efficiency from 11% at 5.0 M to 65% for 0.05 M. Conversely, as regards power density, results show a decrease from 5.6 W/m^2 at 5 M to 1.3 W/m^2 at 0.5 M. The highest power density, equal to 6.4 W/m^2, is observed for 3.6 M. This result is related to the membranes resistance, which approaches a minimum value near 3.6 M.

According to Eqs 17-18, a reduction of salinity gradient reduces both electrical power produced and also osmosis and salt diffusion across the membranes.

The improvements of exergy efficiency when reducing concentrated solution indicate that even though less electrical power is produced, a better exploitation of exergy occurs due to a reduction of the exergy destroyed by uncontrolled mixing phenomena.

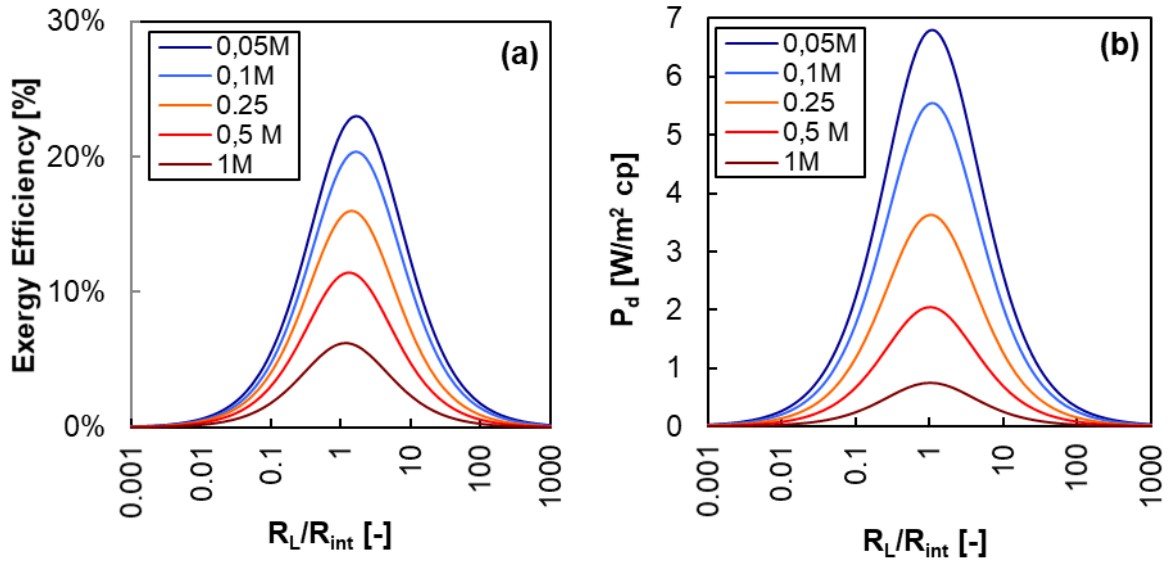

Fig. 12. Exergy efficiency (a) and Power density (b) as function of the R_L/R_{int} ratio and the dilute solution concentration, setting the concentrate concentration at 3.6 M. RED stack 0.1 m x 0.1 m, $v_{conc}=v_{dil}=1$ cm·s^{-1}, scenario D.

As shown in Fig. 12, different results were obtained when the dilute concentration was increased from 0.05 M to 1.00 M, while keeping the concentrate solution at 3.6 M (value maximizing the power). Also, in this case, the reduction in concentration difference produces a decrease of the uncontrolled mixing phenomena, however, the increase of the dilute solution concentration strongly affects OCV values. Indeed, as shown in Eq. 9, OCV is dependent from the logarithm of the ratio between concentrate and dilute solution. Thus, an increase of dilute solution concentration while keeping constant the concentrate solution, affect OCV much more than a decrease in concentrate while keeping constant the dilute concentration. As a consequence, the heavy reduction in OCV drastically reduces the electric power produced by

the unit which is not compensated by the decrease of irreversibility generated by osmosis and salt diffusion.

3.4 Effect of flow arrangement and cell pair length

This section presents a sensitivity analysis to highlight the influence of flow arrangement and cell pair length (L) on RED performance.

The analysis was performed considering counter-current and co-current flow arrangement, varying stack length from 0.1 m to 1.0 m and fixing inlet velocity equal to 1 $cm \cdot s^{-1}$. Concentration values equal to 3.6 M and 0.05 M were considered for concentrate and dilute, respectively.

When changing channel length from 0.1 m to 1.0 m, residence time of solutions within the stack increases. Then, more electrical power is produced by the pile as well more water and salt are exchanged between solutions due to osmosis and salt fluxes.

Considering a stack length less or equal to 0.4 m (i.e. short stack), though for the two flow arrangements a different profile concentration is observed, the value of electrical outputs are practically the same due to low residence time of both stream within the stack. In these cases, flow arrangement does not influence RED exergy performance, which equals to 23 % for both cases. Conversely, when channel length is greater than 0.5 m, concentration profiles along stack length differ for the two cases. In both configurations, the exergy efficiency decreases when increasing the channel length. This trend can be easily explained by means of the following consideration: due to higher residence time within the stack, more electric power is produced as well more irreversibility is generated by uncontrolled mixing phenomena. In these cases, the exergy destruction occuring due to osmosis and salt diffusion is not offset by the increase in electric power generation, thus a decrease of RED performance occurs.

Still, it is possible to observe how the counter-current stack is more performing than the co-current when incresing stack length. As shown in Fig. 13.a and b moving from 0.1 m to 1 m,

exergy destruction is nearly equal for both cases, conversely, power production is greater in counter-current arrangement.

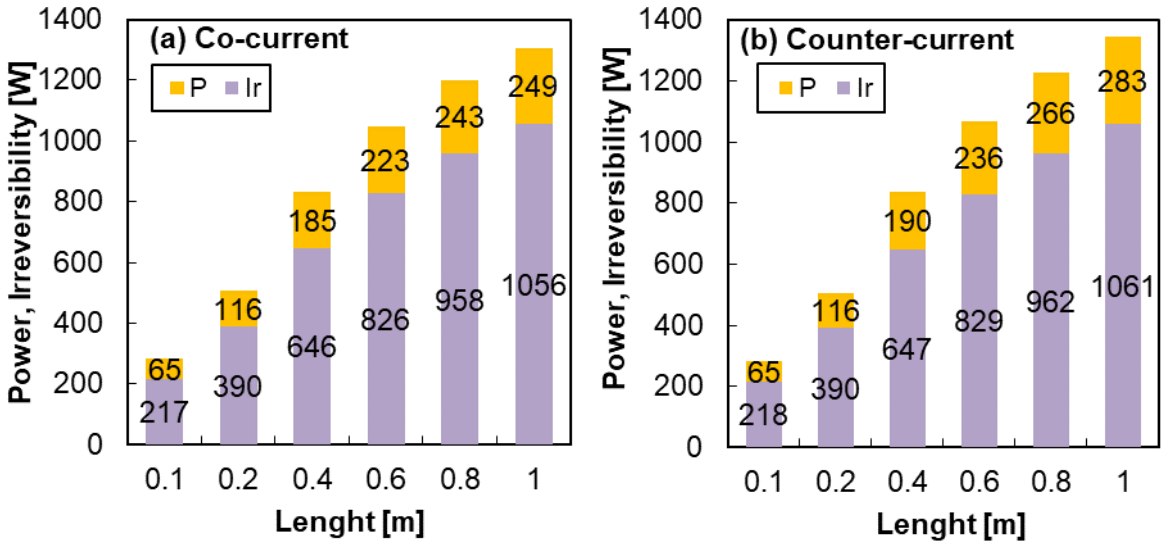

Fig. 13. Power generation and Irreversibility losses in Co-current (a) and Counter-current (b) arrangements. RED stack L m x 0.1 m, C_{conc}=3.6 M C_{dil}=0.05 M, v_{conc}= v_{dil}=1 cm·s^{-1}, scenario D.

3.5 Effect of feed velocity

In this section, the effect of the different residence times on exergy efficiency and gross power is analysed. In the first scenario, the dilute velocity was set at 2 cm/s, while the concentrate velocity is increased from 0.4 cm/s to 2 cm/s. Conversely, in the second scenario, the concentrate velocity was set at 2 cm/s while dilute velocity was varied from 0.4 cm/s to 2 cm/s. As shown in Fig. 14.a, when increasing dilute velocity from 0.4 to 2.0 cm/s, an increase of both power and exergy efficiency is observed. In particular, the exergy efficiency improves from 8.6 % to 22%, while the power increases from 76 W to 440 W. The low residence time of dilute solution within the stack results in a low average dilute concentration. Thus, according to Eq. 9, a significant increase of the electric voltage is observed, with negligible variation of the uncontrolled mixing phenomena.

Conversely, the increase of the concentrate velocity results in a slight increase of power output and a decrease of the exergy efficiency as shown in Fig. 14.b. In particular, increasing concentrate velocity from 0.4 to 2 cm/s, the exergy efficiency decreases from 31% to 22%,

while the power increases from 360 W to 440 W. In this case, the higher average concentration of concentrate along the channels results, in a slight increase in pile electric voltage according to Eq. 9. However, exergy destruction due to uncontrolled mixing phenomena is not balanced by the increase of electric power, leading to a less performing unit results. Interestingly, at very low v_{conc}, η_{ex} reaches the highest value indicating that the reduction of uncontrolled mixing phenomena (due to the much lower average concentration in the channel) dominates the overall efficiency being more important than the reduction of power output also caused by the lower average concentration.

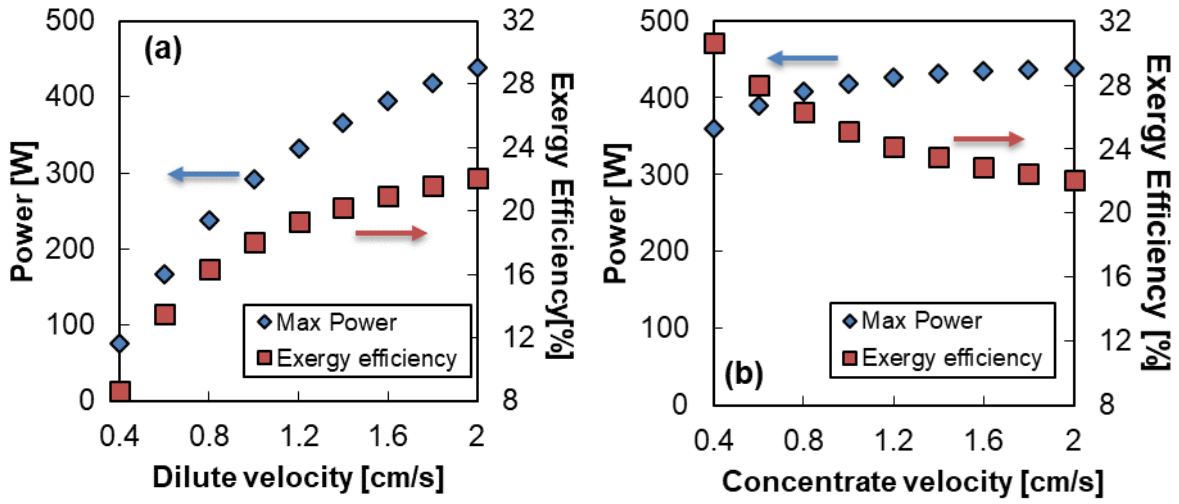

Fig. 14. Maximum power and corresponding exergy efficiency as function of (a) dilute velocity, (setting concentrate velocity at 2 cm·s^{-1}) and (b) concentrate velocity (setting dilute velocity at 2 cm·s^{-1}). RED stack 1 m x 0.1 m Counter-Current arrangement, C_{conc}=3.6 M C_{dil}=0.05 M, scenario D.

4 CONCLUSIONS AND FUTURE REMARKS

Reverse Electrodialysis in closed loop configurations has recently motivated the interest of research and industry thanks to the large potential of applications in the field of energy storage and conversion. One of the main advantage of closed-loop RED is the possible use of a great variety of salinity gradients, in terms of type of salt and operating concentrations and flow rates.

An original exergy analysis of the RED process was carried out in order to investigate RED performance in terms of exergy efficiency and power yield in a wide range of system operations. A mono-dimensional model of the RED process was developed, including also uncontrolled mixing phenomena (arising from the non-ideal behaviour of ion exchange membranes) such as salt and water diffusive flux across membranes.

In particular, water flux due to osmosis has been found to have the most detrimental effect on exergy efficiency when salinity gradient above 2M was adopted, with exergy losses (at maximum Power output conditions) accounting for 60-80% of total losses in the worst scenarios. A less dramatic, yet important effect is associated with diffusive salt flux.

A sensitivity analysis was also carried out in order to assess the influence of operating parameters on process performance. The analysis showed that exergy efficiency heavily increases when decreasing dilute concentration, while it increases when decreasing the salinity of concentrate feed reaching values up to 25% and 60% in the two cases. Power density decreases from values around 6.5 W/m^2_{cp} to slightly above 1 W/m^2_{cp} respectively, due to the salinity gradient reduction across the membranes.

Also, the effect of counter-current and co-current flow arrangement was assessed, indicating how the former leads to better performance only for long-length stack design.

Finally, different residence times for dilute and concentrate were considered in each simulated scenario. Results indicate that exergy efficiency increases for longer residence time in the concentrate channel, while it decreases for shorter residence time in the dilute.

Future work will focus on the extension of exergy analysis to real applications of closed loop RED systems (e.g. RED-Heat Engine) in order to identify optimal design and operating conditions for the enhancement of the overall energetic conversion efficiency of the process. Furthermore, this approach could be easily applied to investigate RED performance for the case of salts other than NaCl.

ACKNOWLEDGEMENTS

This work was performed within the RED-Heat-to-Power project (Conversion of Low Grade Heat to Power through closed loop Reverse Electro-Dialysis), funded by EU within the H2020 research & innovation programme, grant agreement No. 640667. www.red-heat-to-power.eu.

The authors are thankful to FUJIFILM Manufacturing Europe B.V. for providing information on IEMs properties.

NOMENCLATURE

A_{cp}	Area of a cell pair [m^2]
a_s	Salt Activity
a_w	Water Activity
b	Membrane Width (m)
$\dot{B}$	Exergy Flow (W_{ex})
C_{conc}	Concentrate Molar Concentration (M)
C_{dil}	Dilute Molar Concentration (M)
Δx	Discretization length (m)
E_{cell}	Voltage generated by the cell pair (V)
E_{loss}	Ohmic loss due to internal stack resistances (W)
E_{mix}	Exergy destruction due to uncontrolled mixing phenomena (W)
E_{stack}	Voltage generated by the pile (V)
F	Faraday constant (C/mol)
h	Specific enthalpy (kJ/kg)
$\tilde{h}$	Partial Molar Enthalpy of the "i^{th}" species (kJ/kmol)
I	Electric current (A)
IEM	Ionic Exchange Membrane
$I_{r,RED}$	Exergy destruction within RED unit (W)
J	Molar Flux (mol/m^2s)
m	Molality (mol/kg_{solv})
M_s	Salt molecular weight (mol/kg)
M_w	Water molecular weight (mol/kg)
N_{cp}	Number of cell pair
N_k	Number of discretization elements
OCV	Open Circuit Voltage (V)
p	Pressure (kPa)
P_d	Power density (W/m^2)
P_E	Electric Power (W)
P_s	Membrane Permeability to Salt (m^2/s)

P_w	Membrane Permeability to Water (m/Pa·s)
Q	Volumetric Flowrate (m^3/s)
R	Gas constant (J/(K mol))
R_{AEM}	Anionic Membrane Resistance (Ωm^2)
R_{blamk}	Electrical resistance of the electrodic compartment (Ω)
R_{cell}	Electrical resistance of the cell pair (Ω)
R_{CEM}	Cationic membrane Resistance (Ωm^2)
R_{conc}	Electrical resistance of concentrate (Ωm^2)
R_{dil}	Electrical resistance of dilute (Ωm^2)
RED	Reverse Electrodialysis
R_{int}	Internal Stack Resistance (Ω)
R_{L}	Load Resistance (Ω)
R_{u}	Universal constant of gases (kJ/(kmol K))
s	Specific entropy (kJ/(kg K))
$\tilde{s}$	Molar Specific entropy (kJ/kmol)
T	Temperature (°C or K)
v_{conc}	Concentrate Velocity (m/s)
v_{dil}	Dilute Velocity (m/s)
x_{s}	Salt molar fraction (dimensionless)
x_{w}	Water molar fraction (dimensionless)
z	Ion charge

Greek symbols

α	Permselectivity
γ	Salt activity coefficient (dimensionless)
δ_{m}	Membrane Thickness (m)
η	Performance (dimensionless)
μ_{MX}	Chemical potential of the generic solute MX
ρ	Density (kg/m^3)
ϕ	Osmotic Coefficient (dimensionless)

Subscripts

0	Related to reference or “dead” state
in	Related to inlet
M	Related to cation
out	Related to outlet
s	Related to salt
sol	Related to solution
X	Related to anion
w	Related to water

REFERENCES

[1] R.E. Pattle, Production of Electric Power by mixing Fresh and Salt Water in the Hydroelectric Pile, Nature. 174 (1954) 660–660. doi:10.1038/174660a0.

[2] A. Achilli, T.Y. Cath, A.E. Childress, Power generation with pressure retarded osmosis: An experimental and theoretical investigation, J. Memb. Sci. 343 (2009) 42–52. doi:10.1016/j.memsci.2009.07.006.

[3] F. Giacalone, A. Cipollina, F. Grisafi, A. Tamburini, G. Vella, G. Micale, Characterization of pressure retarded osmosis lab-scale systems, Desalin. Water Treat. 57 (2016) 22994–23006. doi:10.1080/19443994.2016.1173379.

[4] R. Audinos, Electrodialyse inverse. Etude de l'energie electrique obtenue a partir de deux solutions de salinites differentes, J. Power Sources. 10 (1983). doi:10.1016/0378-7753(83)80077-9.

[5] J. Veerman, M. Saakes, S.J. Metz, G.J. Harmsen, Reverse electrodialysis: Performance of a stack with 50 cells on the mixing of sea and river water, J. Memb. Sci. 327 (2009) 136–144. doi:10.1016/j.memsci.2008.11.015.

[6] P. Długołecki, P. Ogonowski, S.J. Metz, M. Saakes, K. Nijmeijer, M. Wessling, On the resistances of membrane, diffusion boundary layer and double layer in ion exchange membrane transport, J. Memb. Sci. 349 (2010) 369–379. doi:10.1016/j.memsci.2009.11.069.

[7] D.A. Vermaas, M. Saakes, K. Nijmeijer, Doubled power density from salinity gradients at reduced intermembrane distance, Environ. Sci. Technol. 45 (2011) 7089–7095. doi:10.1021/es2012758.

[8] A. Daniilidis, D.A. Vermaas, R. Herber, K. Nijmeijer, Experimentally obtainable energy from mixing river water, seawater or brines with reverse electrodialysis, Renew. Energy. 64 (2014) 123–131. doi:10.1016/j.renene.2013.11.001.

[9] M. Tedesco, A. Cipollina, A. Tamburini, G. Micale, Towards 1 kW power production in a reverse electrodialysis pilot plant with saline waters and concentrated brines, J. Memb. Sci. 522 (2017) 226–236. doi:10.1016/j.memsci.2016.09.015.

[10] M. Tedesco, C. Scalici, D. Vaccari, A. Cipollina, A. Tamburini, G. Micale, Performance of the first reverse electrodialysis pilot plant for power production from saline waters and concentrated brines, J. Memb. Sci. 500 (2016) 33–45. doi:10.1016/j.memsci.2015.10.057.

[11] A. Tamburini, A. Cipollina, M. Papapetrou, A. Piacentino, G. Micale, 7 – Salinity gradient engines, in: Sustain. Energy from Salin. Gradients, 2016: pp. 219–256. doi:10.1016/B978-0-08-100312-1.00007-9.

[12] A. Tamburini, M. Tedesco, A. Cipollina, G. Micale, M. Ciofalo, M. Papapetrou, W. Van Baak, A. Piacentino, Reverse electrodialysis heat engine for sustainable power production, Appl. Energy. 206 (2017) 1334–1353. doi:10.1016/j.apenergy.2017.10.008.

[13] M. Bevacqua, A. Tamburini, M. Papapetrou, A. Cipollina, G. Micale, A. Piacentino, Reverse electrodialysis with NH4HCO3-water systems for heat-to-power conversion, Energy. (2017). doi:10.1016/j.energy.2017.07.012.

[14] R.S. Kingsbury, K. Chu, O. Coronell, Energy storage by reversible electrodialysis: The concentration battery, J. Memb. Sci. 495 (2015) 502–516. doi:https://doi.org/10.1016/j.memsci.2015.06.050.

[15] W.J. van Egmond, U.K. Starke, M. Saakes, C.J.N. Buisman, H.V.M. Hamelers, Energy efficiency of a concentration gradient flow battery at elevated temperatures, J. Power Sources. 340 (2017) 71–79. doi:https://doi.org/10.1016/j.jpowsour.2016.11.043.

[16] Baobab Project: Blue Acid/Base Battery: Storage and recovery of renewable electrical energy by reversible salt water dissociation. European H200 project. Contract n° 73118,

(n.d.).
[17] T. J. Kotas, The exergy method of thermal plant analysis, Butterworths, 1985. doi:10.1016/S0140-7007(97)85546-6.
[18] E. Sciubba, Enrico, A Critical Interpretation and Quantitative Extension of the Sama-Szargut Second Law Rules in an Extended Exergy Perspective, Energies. 7 (2014) 5357–5373. doi:10.3390/en7085357.
[19] W. Sun, X. Yue, Y. Wang, Exergy efficiency analysis of ORC (Organic Rankine Cycle) and ORC-based combined cycles driven by low-temperature waste heat, Energy Convers. Manag. 135 (2017) 63–73. doi:10.1016/j.enconman.2016.12.042.
[20] F. Ranjbar, A. Chitsaz, S.M.S. Mahmoudi, S. Khalilarya, M.A. Rosen, Energy and exergy assessments of a novel trigeneration system based on a solid oxide fuel cell, Energy Convers. Manag. 87 (2014) 318–327. doi:10.1016/j.enconman.2014.07.014.
[21] A. Vatani, M. Mehrpooya, A. Palizdar, Advanced exergetic analysis of five natural gas liquefaction processes, Energy Convers. Manag. 78 (2014) 720–737. doi:10.1016/j.enconman.2013.11.050.
[22] W.J. Kostowski, J. Kalina, P. Bargiel, P. Szufleński, Energy and exergy recovery in a natural gas compressor station - A technical and economic analysis, Energy Convers. Manag. 104 (2015) 17–31. doi:10.1016/j.enconman.2015.07.002.
[23] A. Noroozian, A. Mohammadi, M. Bidi, M.H. Ahmadi, Energy, exergy and economic analyses of a novel system to recover waste heat and water in steam power plants, Energy Convers. Manag. 144 (2017) 351–360. doi:https://doi.org/10.1016/j.enconman.2017.04.067.
[24] L. Marletta, Luigi, Air Conditioning Systems from a 2nd Law Perspective, Entropy. 12 (2010) 859–877. doi:10.3390/e12040859.
[25] N. Jain, A. Alleyne, Exergy-based optimal control of a vapor compression system, Energy Convers. Manag. 92 (2015) 353–365. doi:10.1016/j.enconman.2014.12.014.
[26] B.A. Qureshi, S.M. Zubair, Exergetic efficiency of NF, RO and EDR desalination plants, Desalination. 378 (2016). doi:10.1016/j.desal.2015.09.027.
[27] B.A. Qureshi, S.M. Zubair, Exergy and sensitivity analysis of electrodialysis reversal desalination plants, Desalination. 394 (2016). doi:10.1016/j.desal.2016.05.015.
[28] N. Kahraman, Y. A. Cengel, Exergy analysis of a MSF distillation plant, Energy Convers. Manag. 46 (2005) 2625–2636. doi:10.1016/j.enconman.2004.11.009.
[29] A. Piacentino, Application of advanced thermodynamics, thermoeconomics and exergy costing to a Multiple Effect Distillation plant: In-depth analysis of cost formation process, Desalination. 371 (2015). doi:10.1016/j.desal.2015.06.008.
[30] C.A. Frangopoulos, Exergy, Energy System Analysis and Optimization - Volume I: Exergy and Thermodynamic Analysis, EOLSS Publications, 2009.
[31] A. Valero, C.T. Cuadra, Thermoeconomic Analysis, in: C. Frangopoulos (Ed.), Exergy, Energy Syst. Anal. Optim., Oxford: EOLSS Publishers, 2004.
[32] V. Verda, M. Caccin, A. Kona, Thermoeconomic cost assessment in future district heating networks, Energy. 117 (2016) 485–491. doi:https://doi.org/10.1016/j.energy.2016.07.016.
[33] A. Piacentino, F. Cardona, On thermoeconomics of energy systems at variable load conditions : Integrated optimization of plant design and operation, 48 (2007) 2341–2355. doi:10.1016/j.enconman.2007.03.002.
[34] A. Valero, L. Serra, J. Royo, Structural theory and thermoeconomic diagnosis Part I . On malfunction and dysfunction analysis, 43 (2002) 1503–1518.
[35] J. Szargut, A. Ziębik, W. Stanek, Depletion of the non-renewable natural exergy resources as a measure of the ecological cost, Energy Convers. Manag. 43 (2002) 1149–1163. doi:https://doi.org/10.1016/S0196-8904(02)00005-5.

[36] R. e L. Cornelissen, G.G. Hirs, The value of the exergetic life cycle assessment besides the LCA, Energy Convers. Manag. 43 (2002) 1417–1424.
[37] M.V. Rocco, Primary exergy cost of goods and services : an input-output approach, Springer, 2016.
[38] M. V Rocco, A. Di Lucchio, E. Colombo, Exergy Life Cycle Assessment of electricity production from Waste-to-Energy technology: A Hybrid Input-Output approach, Appl. Energy. 194 (2017) 832–844. doi:https://doi.org/10.1016/j.apenergy.2016.11.059.
[39] J. Veerman, R.M. de Jong, M. Saakes, S.J. Metz, G.J. Harmsen, Reverse electrodialysis: Comparison of six commercial membrane pairs on the thermodynamic efficiency and power density, J. Memb. Sci. 343 (2009) 7–15. doi:10.1016/j.memsci.2009.05.047.
[40] J. Veerman, M. Saakes, S.J. Metz, G.J. Harmsen, Reverse electrodialysis: A validated process model for design and optimization, Chem. Eng. J. 166 (2011) 256–268. doi:10.1016/j.cej.2010.10.071.
[41] N.Y. Yip, D.A. Vermaas, K. Nijmeijer, M. Elimelech, Thermodynamic, energy efficiency, and power density analysis of reverse electrodialysis power generation with natural salinity gradients, Environ. Sci. Technol. 48 (2014) 4925–4936. doi:10.1021/es5005413.
[42] D.A. Vermaas, J. Veerman, N.Y. Yip, M. Elimelech, M. Saakes, K. Nijmeijer, High efficiency in energy generation from salinity gradients with reverse electrodialysis, ACS Sustain. Chem. Eng. 1 (2013) 1295–1302. doi:10.1021/sc400150w.
[43] N.Y. Yip, M. Elimelech, Thermodynamic and energy efficiency analysis of power generation from natural salinity gradients by pressure retarded osmosis, Environ. Sci. Technol. 46 (2012) 5230–5239. doi:10.1021/es300060m.
[44] K. S.A., Engineering equation solver, (2010).
[45] T.Z. Fahidy, Activity coefficients in electrolyte solutions (second edition), edited by Kenneth S. Pitzer, 1991, 542 + vi pages, CRC Press, Boca Raton, FL; ISBN 0-8493-5415-3. Price: US$ 195.00, Can. J. Chem. Eng. 71 (1993) 494–494. doi:10.1002/cjce.5450710328.
[46] K.S. Pitzer, J.C. Peiper, R.H. Busey, Thermodynamic Properties of Aqueous Sodium Chloride Solutions, J. Phys. Chem. Ref. Data. 13 (1984) 1–102. doi:10.1063/1.555709.
[47] D.G. Archer, Thermodynamic propertis of the KCl + H2O system, J. Phys. Chem. Ref. Data. 28 (1999) 1–16. doi:10.1063/1.556034.
[48] T. Isono, Measurements of density, viscosity, and electrolytic conductivity of concentrated aqueous electrolyte solutions - 1. LiCl, NaCl, KCl, RbCl, CsCl, MgSO4, ZnSO4 AND NiSO4., Rika Gaku Kenkyujo Hokoku. 56 (1980).
[49] M. Tedesco, A. Cipollina, A. Tamburini, I.D.L. Bogle, G. Micale, A simulation tool for analysis and design of reverse electrodialysis using concentrated brines, Chem. Eng. Res. Des. 93 (2015) 441–456. doi:10.1016/j.cherd.2014.05.009.
[50] M. Tedesco, A. Cipollina, A. Tamburini, I.D.L. Bogle, G. Micale, A simulation tool for analysis and design of reverse electrodialysis using concentrated brines, Chem. Eng. Res. Des. 93 (2015) 441–456. doi:10.1016/j.cherd.2014.05.009.
[51] L. Gurreri, M. Ciofalo, A. Cipollina, A. Tamburini, W. Van Baak, CFD modelling of profiled-membrane channels for Reverse Electrodialysis, (2014). doi:10.1080/19443994.2014.940651.
[52] L. Gurreri, A. Tamburini, A. Cipollina, G. Micale, M. Ciofalo, Flow and mass transfer in spacer-filled channels for reverse electrodialysis: a CFD parametrical study, J. Memb. Sci. 497 (2016) 300–317. doi:10.1016/j.memsci.2015.09.006.
[53] L. Gurreri, A. Tamburini, A. Cipollina, G. Micale, M. Ciofalo, Pressure drop at low Reynolds numbers in woven-spacer-filled channels for membrane processes : CFD prediction and experimental validation, 61 (2017) 170–182.

doi:10.5004/dwt.2016.11279.
[54] S. Pawlowski, J.G. Crespo, S. Velizarov, Pressure drop in reverse electrodialysis : Experimental and modeling studies for stacks with variable number of cell pairs, J. Memb. Sci. 462 (2014) 96–111. doi:10.1016/j.memsci.2014.03.020.
[55] R.W. Baker, 2 Membrane Transport Theory, in: Membr. Technol. Appl., 2004: pp. 15–87. doi:10.1002/0470020393.ch2.
[56] M. Tedesco, E. Brauns, A. Cipollina, G. Micale, P. Modica, G. Russo, J. Helsen, Reverse electrodialysis with saline waters and concentrated brines: A laboratory investigation towards technology scale-up, J. Memb. Sci. 492 (2015) 9–20. doi:10.1016/j.memsci.2015.05.020.
[57] M. Micari, M. Bevacqua, A. Cipollina, A. Tamburini, W. Van Baak, T. Putts, G.M. Micale, Effect of different aqueous solutions of pure salts and salt mixtures in reverse electrodialysis systems for closed-loop applications, J. Memb. Sci. in press (2018).
[58] A. Bejan, Advanced engineering thermodynamics, J. Wiley & Sons, 1997. https://books.google.co.uk/books?id=D-NSAAAAMAAJ.
[59] J. Szargut, Exergy Method: Technical and Ecological Applications., UK: WIT Press, 2005.
[60] J. Veerman, D.A. Vermaas, 4 – Reverse electrodialysis: Fundamentals, in: Sustain. Energy from Salin. Gradients, 2016: pp. 77–133. doi:10.1016/B978-0-08-100312-1.00004-3.